

MRK 71 / NGC 2366: THE NEAREST GREEN PEA ANALOG

GENOVEVA MICHEVA¹, M. S. OEY¹, ANNE E. JASKOT², AND BETHAN L. JAMES³
(Accepted 24 July 2017)

¹University of Michigan, 311 West Hall, 1085 S. University Ave, Ann Arbor, MI 48109-1107, USA

²Department of Astronomy, Smith College, Northampton, MA 01063, USA

³STScI, 3700 San Martin Drive, Baltimore, MD 21218, USA

ABSTRACT

We present the remarkable discovery that the dwarf irregular galaxy NGC 2366 is an excellent analog of the Green Pea (GP) galaxies, which are characterized by extremely high ionization parameters. The similarities are driven predominantly by the giant H II region Markarian 71 (Mrk 71). We compare the system with GPs in terms of morphology, excitation properties, specific star-formation rate, kinematics, absorption of low-ionization species, reddening, and chemical abundance, and find consistencies throughout. Since extreme GPs are associated with both candidate and confirmed Lyman continuum (LyC) emitters, Mrk 71/NGC 2366 is thus also a good candidate for LyC escape. The spatially resolved data for this object show a superbubble blowout generated by mechanical feedback from one of its two super star clusters (SSCs), Knot B, while the extreme ionization properties are driven by the $\lesssim 1$ Myr-old, enshrouded SSC Knot A, which has ~ 10 times higher ionizing luminosity. Very massive stars ($> 100 M_{\odot}$) may be present in this remarkable object. Ionization-parameter mapping indicates the blowout region is optically thin in the LyC, and the general properties also suggest LyC escape in the line of sight. Mrk 71/NGC 2366 does differ from GPs in that it is 1 – 2 orders of magnitude less luminous. The presence of this faint GP analog and candidate LyC emitter (LCE) so close to us suggests that LCEs may be numerous and commonplace, and therefore could significantly contribute to the cosmic ionizing budget. Mrk 71/NGC 2366 offers an unprecedentedly detailed look at the viscera of a candidate LCE, and could clarify the mechanisms of LyC escape.

1. INTRODUCTION

Lyman continuum (LyC) radiation from star-forming (SF) galaxies escapes into the intergalactic medium (IGM) and contributes to the ionizing budget of the Universe. A key point of interest is to identify the mechanisms of escape and how the properties of the IGM and the emitting galaxy govern the LyC escape fraction (f_{esc}). Ideally, this requires the detection of LyC emitters (LCEs), located close enough to be spatially resolved and studied in detail, as well as statistically large LCE samples from galaxy populations at different redshifts.

At low redshifts the direct detection of LCEs has been notoriously difficult, resulting mostly in upper limits (e.g. [Leitherer et al. 1995](#); [Steidel et al. 2001](#); [Siana et al. 2007, 2015](#); [Vanzella et al. 2010](#)), with a handful of confirmed LyC detections: Haro 11 ($f_{\text{esc}} \sim 3.3\%$; [Leitet et al. 2011](#)), Tol 1247-232 ($f_{\text{esc}} \sim 4.5\%$; [Leitet et al. 2013](#); [Leitherer et al. 2016](#)), Mrk 54 ($f_{\text{esc}} \sim 2.5\%$; [Leitherer et al. 2016](#)), and J0921+4509 ($f_{\text{esc}} \sim 1\%$; [Borthakur et al. 2014](#)). At high redshifts statistically significant samples are easier to obtain; however, the problem of foreground contamination and the severe attenuation of LyC by the IGM has resulted in many non-detections (e.g. [Siana et al. 2015](#); [Vanzella et al. 2015](#); [Guaia et al. 2016](#); [Micheva et al. 2017](#)), with few con-

firmed LCEs ([de Barros et al. 2016](#); [Shapley et al. 2016](#)).

Recently, a new subclass of local compact emission-line galaxies, the Green Peas (GPs; [Cardamone et al. 2009](#)), has been proposed, not only as an excellent analog class of high redshift strongly star-forming galaxies like Lyman alpha emitters (LAEs), but also as strong candidates for LyC emission ([Jaskot & Oey 2013](#)). That the extreme GPs are viable LCE candidates has been dramatically confirmed by [Izotov et al. \(2016a,b\)](#), who spectroscopically observed five GPs at redshifts $z \sim 0.3$ with the Hubble Space Telescope (HST). In all five of their target objects, they directly detect strong LyC emission in the range $f_{\text{esc}} = 6\text{--}13\%$. These are the highest escape fractions measured to date among low-redshift SF galaxies. Note that with the detections by Izotov et al., the number of confirmed LyC leakers at low redshifts has now doubled. The GP class therefore offers a plethora of strong LCE candidates.

GPs are a rare class of low-metallicity, vigorously star-forming galaxies ([Cardamone et al. 2009](#); [Izotov et al. 2011](#)). In the “BPT” diagram of [Baldwin et al. \(1981\)](#) with $\log([\text{NII}]/\text{H}\alpha)$ vs. $\log([\text{OIII}]/\text{H}\beta)$ they occupy the most extreme end of low-mass, low-metallicity local SF galaxies in the Sloan Digital Sky survey (SDSS). They are defined by $[\text{OIII}]\lambda 5007$ emission-line equivalent widths exceeding hundreds of \AA ([Cardamone et al.](#)

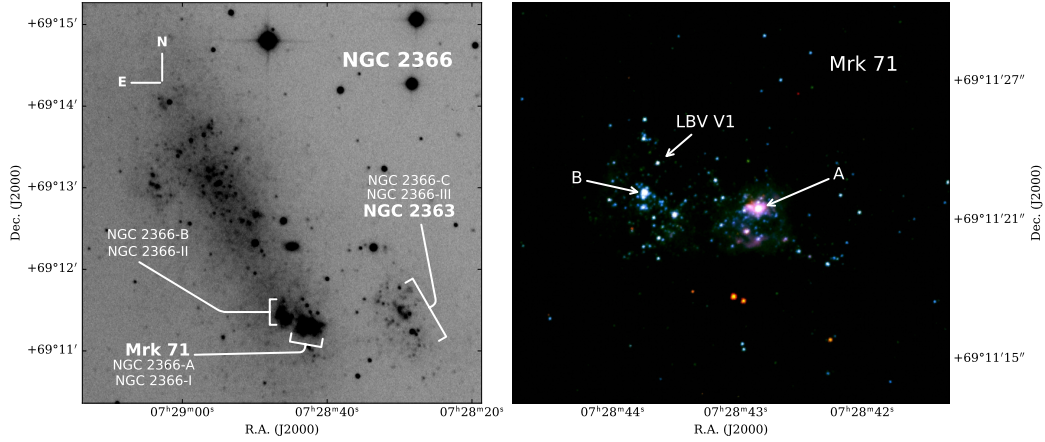


Figure 1. Left: R -band image (Dale et al. 2009) of the NGC 2366 system, including NGC 2366 and neighboring galaxy NGC 2363. The giant H II region Mrk 71 is identified at the south end of NGC 2366. Mrk 71 is often erroneously referred to as “NGC 2363” or “NGC 2363-A”. Some designations from the literature are shown: NGC 2366-I, -II, -III are from Drissen et al. (2000), and NGC 2366-A, -B, -C are from Roy et al. (1991). Right: Color composite from archive *HST*/WFC3 broad band imaging of Mrk 71 (James et al. 2016) with (red, green, blue) = (F814W, F547M, F336W), showing the positions of Knots A and B.

2009). At their typical redshift of $z \sim 0.2$ this emission falls into the Sloan r band and dominates the luminosity of the 3-color gri image. They have sub-solar metallicities (Amorín et al. 2010, 2012a; Hawley 2012), compact morphology, and some of the highest specific star formation rates (sSFR) in the local Universe. Henry et al. (2015) show that GPs are similar to high redshift galaxies in terms of having double-peaked Ly α profiles, with velocity separations indicative of low HI column densities, and Ly α luminosities and equivalent widths in the range of most high redshift LAEs. GPs have extremely high ionization parameters, as indicated by their [OIII] λ 5007/[O II] λ 3727 ratios, which are some of the highest among local galaxies. In terms of ionization properties GPs are therefore comparable to high redshift LAEs (Nakajima & Ouchi 2014). GPs are therefore a vital population for understanding which galaxies and which physical conditions are responsible for the release of LyC radiation into the intergalactic medium, and ultimately, for cosmic reionization.

We have made a serendipitous discovery of the nearest LCE candidate and GP analog, conveniently located at only 3.4 Mpc (Tolstoy et al. 1995). This object is the dwarf irregular galaxy NGC 2366, whose star formation is strongly dominated by the giant H II region Markarian 71 (Mrk 71). This system is not only consistent with various properties of the GP class, but also is often more extreme than known LCE GPs, which suggests that it is a strong LCE candidate. NGC 2366 is close enough to study in great detail, at a level unprecedented for other GPs or even local LCEs, since it is 25 times closer than the nearest confirmed LCE (Haro 11 at 84.3 Mpc). Given the spatial detail with which we can examine this object, Mrk 71 may clarify mechanisms for LyC escape. In this introductory paper, we establish the similarities between the GPs and NGC 2366, with a focus on the

dominant H II region Mrk 71, as well as examine the likelihood of LyC escape. We will examine the physical processes in Mrk 71 in a subsequent work.

1.1. Nomenclature

NGC 2366 is a Magellanic barred irregular galaxy of class IB(s)m (de Vaucouleurs et al. 1991). There is unfortunate confusion with multiple, and erroneous, nomenclature relating to Mrk 71 and its neighboring complexes, so in Figure 1 we present NGC 2366 with the main substructures indicated with their correct designations. In the left panel of the figure, the large, luminous H II region complex located to the south is Mrk 71. The structure to the west of Mrk 71 is another dwarf galaxy, NGC 2363, interacting with NGC 2366. The right panel of Figure 1 shows a zoom on Mrk 71, with its two prominent super star clusters (SSCs), named A and B by Gonzalez-Delgado et al. (1994), indicated in the figure. We will refer to these identifications for all of our work.

Unfortunately, Mrk 71 has often been mis-identified as NGC 2363 (e.g., Kennicutt et al. 1980; Gonzalez-Delgado et al. 1994; Izotov et al. 1997; Drissen et al. 2000; Hunter et al. 2001; Leitherer et al. 2011), whereas in fact, the latter is the neighboring galaxy to the west of Mrk 71 in Figure 1a (Corwin 2006). This mislabeling has propagated into the naming of the two SSCs in Mrk 71, i.e., clusters A and B are sometimes called “NGC 2363-A” and “NGC 2363-B” (e.g., Gonzalez-Delgado et al. 1994; Drissen et al. 2000; Leitherer et al. 2011).

To aid cross-referencing, we also indicate alternative designations in Figure 1. The three most prominent substructures associated with NGC 2366 have been labeled NGC 2366-I (=Mrk 71), NGC 2366-II (bright H II region to the north-east of Mrk 71), and NGC 2366-III (=NGC 2363) by Drissen et al. (2000). These same structures

were instead referred to as NGC 2366-A, NGC 2366-B, and NGC 2366-C by Roy et al. (1991).

Figure 1 is representative of our attempt to revert to the original nomenclature in order to clear up the confusion around the different naming conventions used in the literature. We will refer to the parent galaxy only as NGC 2366, to its brightest HII region only as Mrk 71, and to the two SSCs in Mrk 71 as Knot A and Knot B throughout this paper. We refer to the entire combined ensemble of NGC 2366 including Mrk 71 and NGC 2366-II, plus NGC 2363, as the “NGC 2366 system”.

2. NGC 2366 AS A GREEN PEA ANALOG

The HII region Mrk 71 has been extensively studied in the literature both on its own merit and as part of the larger host galaxy NGC 2366 (e.g. Masegosa et al. 1991; Roy et al. 1992; Gonzalez-Delgado et al. 1994; Izotov et al. 1997; Drissen et al. 2000; Noeske et al. 2000; Izotov & Thuan 2011; Thuan et al. 2014; James et al. 2016). We will demonstrate that this system shares the key properties of GPs and Lyman-break analogs (LBAs), making it a unique local analog of GPs, as well as a strong LCE candidate. To facilitate the comparison with these galaxy classes, we define these comparison samples below.

The “average” GP sample: GPs were first introduced by Cardamone et al. (2009), who selected the galaxies by eye from the Galaxy Zoo forum to be “compact” and “green” in the SDSS g , r , i composite images. The properties of this sample that emerged through their analysis of SDSS spectra revealed an average redshift of $z \sim 0.2$, extremely high equivalent width of [OIII] $\lambda\lambda 4959, 5007$, sub-solar metallicities, low masses, and high star formation rates. This sample has been subsequently well studied and re-analysed by, for example, Izotov et al. (2011), who provide updated stellar masses; Hawley (2012), who give detailed abundances; and Henry et al. (2015) who examine the Ly α properties. We refer to properties of the Cardamone samples as those of the “average” GP sample throughout this paper. The wide range of ionization properties of the average GPs implies that some but not all GPs in this sample are expected to be LCE candidates.

The “extreme” GP sample: Jaskot & Oey (2013) suggest that GPs with extreme ionization properties are good candidates for LyC emission. They assemble a subsample of extreme GPs characterized by high ratios of [O III]/[O II] $\gtrsim 7$, and suggest that such high ratios result from either an unusually high ionization parameter, or alternatively, a less extreme ionization parameter in combination with low optical depth. While Stasińska et al. (2015) show that high line ratios alone do not necessarily imply massive escape of LyC, the discovery of five LyC leaking GPs through direct detection by Izotov et al. (2016a,b) does indeed suggest that GPs with extreme ionization properties make for excellent LCE candidates. Throughout this paper we refer to the sample of “extreme” GPs as that defined by the properties of

the GPs in Jaskot & Oey (2013), combined with the five confirmed LyC emitting GPs of Izotov et al. (2016a,b).

The LBA sample: Another class of local analogs to star-forming high-redshift galaxies are the LBAs (Heckman et al. 2005; Overzier et al. 2009, 2010), selected to be the most UV luminous ($L_{\text{FUV}} > 10^{10.3} L_{\odot}$), and most compact ($I_{\text{FUV}} > 10^9 L_{\odot} \text{kpc}^{-2}$) star-forming galaxies at redshift $z < 0.3$ (e.g. Heckman et al. 2005; Hoopes et al. 2007; Overzier et al. 2008). LBAs are of interest because some have been confirmed as LCEs (Borthakur et al. 2014), while others are good LCE candidates (Heckman et al. 2011). While they are on average more massive (stellar mass $M_{\star} = 1\text{--}50 \times 10^9 M_{\odot}$) and metal rich ($Z = 0.13\text{--}2.5 Z_{\odot}$, Heckman et al. 2001) than GPs, at the metal-poor low-mass end of the LBA distribution they overlap with GPs, and several of the GPs in Cardamone et al. (2009) are among the LBAs in Overzier et al. (2009). Heckman et al. (2011) infer a relative $f_{\text{esc}} = 4\text{--}12\%$ (assuming a dust-free case) from the residual core intensity of strong UV absorption lines for three of their eight LBAs. This indirect technique of detecting LCE candidates was validated by Borthakur et al. (2014), who spectroscopically observe an absolute $f_{\text{esc}} = 1\%$ from a $z \sim 0.2$ LBA, selected from the three candidates in Heckman et al. (2011). Note that the LCE LBAs are found in the SF-AGN composite region in the BPT diagram (Figure 2); however, no convincing AGN signatures have been detected in these galaxies (Overzier et al. 2009). However, reminiscent of the compact nature of GPs, many LBAs are characterized by the presence of a dominant compact object, strong outflow velocities, and high star formation rates.

There is one important distinction between the host galaxy NGC 2366 and these comparison samples. NGC 2366 has stellar mass $2.6 \pm 0.3 \times 10^8 M_{\odot}$ (Lelli et al. 2014), and $\log(L_{\text{FUV}}[L_{\odot}]) = 8.34$ (McQuinn et al. 2015), with Mrk 71 likely dominating this emission. This stellar mass is ~ 4 times lower than the typical values in the average GP sample ($M_{\star} \sim 11 \times 10^8 M_{\odot}$; Izotov et al. 2011), while the luminosity is two orders of magnitude lower than the average for GPs ($\log(L_{\text{FUV}}[L_{\odot}]) \sim 10.5$; Cardamone et al. 2009). The LBA sample is brighter and more massive than the average GPs, so the differences there are even greater. As a GP analog and LCE candidate, NGC 2366 therefore probes the previously unexplored region of extremely faint and low-mass GPs and LCEs. Aside from its much smaller scale, we now show that the starburst properties of NGC 2366, driven by Mrk 71, are fully consistent with GPs.

Mrk 71 is strongly dominated by two SSCs, Knot A and Knot B. As seen in Figure 1b, the latter is fully exposed, and, while the stars are not fully resolved, its stellar population has been spectroscopically evaluated with both ground-based observations (Gonzalez-Delgado et al. 1994; Sokal et al. 2016) and with *HST*/FOS (Drissen et al. 2000, see §2.10). In contrast, the spectrum of Knot A shows no stellar photospheric features at all. The spectrum is dominated by

strong nebular continuum, including an inverse Balmer break (Gonzalez-Delgado et al. 1994; Drissen et al. 2000), suggesting that the SSC in Knot A is still embedded in its natal cloud. Further supporting evidence comes from Sokal et al. (2016), who find that the radio inferred ionizing flux is considerably larger than that inferred from the optical, which suggests that the cluster has still not fully emerged. Nevertheless, Knot A appears to be responsible for most of the total ionizing luminosity in Mrk 71. This was shown by Drissen et al. (2000), who estimate the number of OB stars in Knot B from spectral synthesis models of *HST*/FOS UV spectra, obtaining the ionizing photon emission rate per second, $\log N_{\text{LyC}} = 50.78$. This implies an $\text{H}\alpha$ luminosity for Knot B of $L(\text{H}\alpha) = 9.1 \times 10^{38} \text{ erg s}^{-1}$. From $\text{H}\alpha$ imaging with *HST*/WFC3, James et al. (2016) obtain a total luminosity for Mrk 71 of $L(\text{H}\alpha) = 8.4 \times 10^{39} \text{ erg s}^{-1}$. Assuming Case B recombination (but see §3) or a uniform, single LyC escape fraction between Knots A and B, Knot B therefore contributes only $\sim 11\%$ to the total ionizing budget of Mrk 71, leaving Knot A as the strongly dominant source for the remaining LyC radiation. As we will show, Knot A also turns out to drive most of the other features linking Mrk 71, and its parent galaxy NGC 2366, to GPs and LCE candidates.

In what follows, we examine a variety of parameters to compare Mrk 71/NGC 2366 to GPs, demonstrating a remarkable correspondence. We summarize these properties in Table 1.

2.1. Morphology

Extreme GPs are compact objects. At their distances, their bright, dominant starbursts are barely resolved with *HST*, but in some objects extended structures are detected. The dominant compact regions have typical effective radii of $r_{1/2} = 0.3\text{--}0.7 \text{ kpc}$ (Jaskot et al. in prep). While it appears more extended than GPs, the Mrk 71 complex would dominate the luminosity of NGC 2366 if viewed at GP distances, and at wavelengths in which GPs are selected. The apparent diameter of Mrk 71 along the major axis is $\sim 20'' \simeq 330 \text{ pc}$. In the redshift range of GPs, $z \simeq 0.03$ to 0.3 , Mrk 71 would therefore have an apparent size of $0.6''$ to $0.07''$, respectively, and mimic the appearance of GPs at SDSS resolution. At the same redshifts, the host galaxy NGC 2366 will have $r_{1/2} = 4.5''$ and $0.6''$, respectively, with Mrk 71 dominating in brightness in the UV. From archival GALEX data we measure an NUV surface brightness for Mrk 71, NGC 2366-II, and the nearby dwarf NGC 2363 (Figure 1) combined, totaling $5.1 \times 10^{-17} \text{ erg s}^{-1} \text{ cm}^{-2} \text{ \AA}^{-1} \text{ arcsec}^{-2}$. This is comparable to the average value for the extended structures that we find around 17 extreme GPs from *HST*/COS NUV acquisition images, $6.6 \times 10^{-17} \text{ erg s}^{-1} \text{ cm}^{-2} \text{ \AA}^{-1} \text{ arcsec}^{-2}$. Over the rest of NGC 2366 the NUV surface brightness is on average an order of magnitude lower, 5.0×10^{-18} , which indicates that, moved to GP redshifts, only the extended region of Mrk 71 plus NGC 2366-II would likely

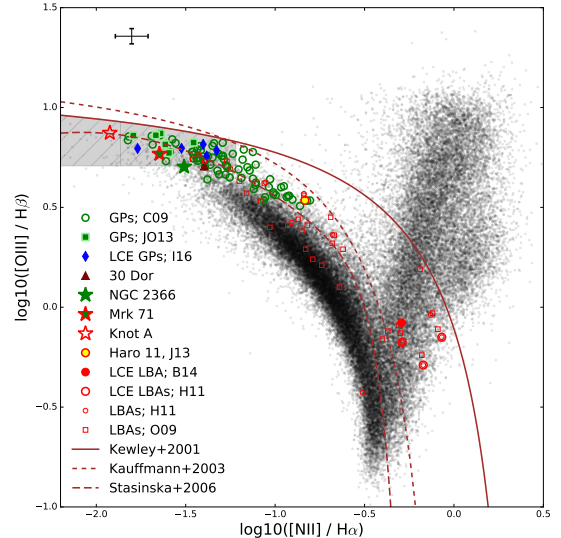


Figure 2. BPT diagram showing the “average GPs” from Cardamone et al. (2009, C09) with open green circles, the “extreme GPs” which are also LCE candidates from Jaskot & Oey (2013, JO13) with filled green squares, the confirmed LCE GPs from Izotov et al. (2016a,b, I16) with filled blue diamonds, LBAs from Overzier et al. (2009, O09) with open red squares and those from Heckman et al. (2011, H11) with thin open red circles. The three unconfirmed LCE LBAs are marked with thick open red circles and the confirmed LCE LBA from Borthakur et al. (2014) with a filled red circle. 30 Dor (Peimbert 2003) and the LCE Haro 11 (data from James et al. 2013, J13) are shown for comparison. The extreme GPs occupy the far end of the low-mass low-metallicity star-forming branch, and are used to define the filled gray region of extreme GP properties. The size of this region includes the uncertainties of the measurements.

be visible in the NUV, with the rest of NGC 2366 below the detection level. This compact appearance is consistent with GPs. Interestingly, even with the remarkable spatial resolution visible in Mrk 71, the dominant object, Knot A, remains strongly characterized by its compactness. It is still barely resolved with the *HST*, and has an estimated upper limit in size of $\text{FWHM} < 2.3 \text{ pc}$ (Thuan & Izotov 2005) for the compact nebula.

Many LBAs are similarly characterized by a dominant central object (DCO, Overzier et al. 2010) with typical $r_{1/2} \sim 150 \text{ pc}$, while the extended host galaxies have a range of optical effective radii $0.48\text{--}4.6 \text{ kpc}$ (Overzier et al. 2009). NGC 2366 has a *B*-band effective radius consistent with LBAs, $r_{1/2} = 2.7 \pm 0.1 \text{ kpc}$ (Hunter et al. 2001).

2.2. Excitation

One of the primary characteristics of the GPs is their high nebular excitation. While GPs are identified based on their high $[\text{O III}]\lambda 5007$ equivalent widths (Cardamone et al. 2009, see below), extreme $[\text{OIII}]\lambda 5007, 4959 / [\text{OII}]\lambda 3727$ line ratios, indicative of correspondingly high ionization parameters, are used as the main characteristic for selecting the extreme GPs in Jaskot & Oey (2013). The latter have ratios of 9–14. The confirmed LCE GPs from Izotov et al. (2016a,b)

have a ratio range of 6.4–8.9, so with their addition to the extreme sample, our combined comparison regime for this ratio is 6 – 14, shown in Table 1. Since this is the defining characteristic of the extreme GP sample, it is of great interest to evaluate this quantity for our local GP analog. From high resolution HST data for Mrk 71 of [OIII] λ 5007 and [OII] λ 3727 obtained by James et al. (2016), we estimate [OIII] λ 5007, 4959/[OII] λ 3727 = 11.7, taking λ 5007/ λ 4959 = 3.0. This ratio is well within the extreme GP range.

To make a first-order estimate of the integrated [O III]/[O II] for the entire NGC 2366 system, we combine the contributions from the rest of the components as follows, weighting by the H α luminosity. The observed [OIII]/[OII] \sim 7.2 for Mrk 71 and 2366-II combined, as measured by (Moustakas & Kennicutt 2006) from drift-scanned, ground-based spectra. We again corrected for the contribution of λ 4959, and we additionally corrected for internal reddening using $C(H\beta) = 0.13$ (§ 2.6) because the published value only accounted for Galactic extinction. We similarly treated the observed ratio for NGC 2363, which was also observed by Moustakas & Kennicutt (2006), obtaining [OIII] λ 5007, 4959/[OII] = 1.08. For the rest of NGC 2366, we adopt mean values of HII regions in the Small Magellanic Cloud (SMC), since the SMC has a similarly low metal abundance as NGC 2366. For the 10 H II regions reported by Dufour & Harlow (1977), the mean of [OIII] λ 5007, 4959/[OII] = 5.56. The relative contributions of Mrk 71 and NGC 2366-II, NGC 2363, and the extended body of NGC 2366 to the total H α luminosity are 0.76, 0.10, and 0.14, respectively, as measured from the H α image published by Dale et al. (2009). Thus, weighting the contributions from all nebular components accordingly, the total mean ratio for the integrated NGC 2366 system is [OIII] λ 5007, 4959/[OII] = 6.34, which is consistent with extreme GPs.

It is apparent that because Mrk 71 strongly dominates the H α luminosity of NGC 2366, it similarly dominates the rest of the integrated nebular properties of the system. Therefore, both the integrated NGC 2366 system and Mrk 71 alone are consistent, not only with the average GPs, but also with the extreme GP sample. We note that, on its own, the dominant source of ionization in Mrk 71, Knot A, strongly outperforms the most extreme GPs in our comparison sample, with a ratio of [OIII]/[OII] = 23.0 ± 0.6 (Gonzalez-Delgado et al. 1994). Thus, the manifestation of a high excitation ratio depends on both extreme excitation of the dominant starburst and dilution by additional star-forming regions in the unresolved system. Our values for all the components are given in Table 1, together with those for the comparison samples.

Further evidence of high ionization is the presence of doubly ionized helium, He II λ 4686, detected both in average GPs (Hawley 2012) and extreme GPs (Jaskot & Oey 2013), with detection rates of \sim 7% and \sim 50%, respectively, and comparable line strengths in the range

He II λ 4686/H β \sim 1–2%. The extreme GP sample contains the confirmed LCE GPs from Izotov et al. (2016a,b); however, these authors do not report He II λ 4686 measurements. Considering only the six extreme GPs of (Jaskot & Oey 2013), for which He II λ 4686 measurements exist, five out of six of these show positive detections. Thus, the detection of this line in extreme GPs appears to be more common than among average GPs. We note that the line emission is narrow, FWHM \sim 3–5 Å (Jaskot & Oey 2013), and therefore likely nebular in nature, as expected for conditions with extreme ionization parameter.

For Mrk 71, James et al. (2016) obtain He II λ 4686/H β = 0.026 from HST/WFC3 narrowband data. This emission is largely due to ionization from Knot B, where the presence of Wolf-Rayet (WR) stars has been confirmed (Drissen et al. 2000, § 2.10). Knot A in Mrk 71 generates He II λ 4686/H β = 0.009 ± 0.001 (Izotov et al. 1997; James et al. 2016). For the integrated NGC 2366 system, we assume the only signal comes from Mrk 71, with the rest of the system contributing zero to the diluted ratio. Applying the same H α -based weights as before, we obtain He II λ 4686/H β \sim 0.019. In terms of the presence and strength of this high-excitation line, NGC 2366 is therefore consistent with the extreme GP sample. The nature of the He II λ 4686 emission and the WR population is further discussed in § 2.9.

The average GP sample occupies the low-mass, low-metallicity region of the BPT diagram, with line ratios $\log([OIII]\lambda 5007/H\beta) \gtrsim 0.5$ and $\log([NII]\lambda 6584/H\alpha) \lesssim -0.8$; while the extreme GPs are found at the end of the distribution, illustrated by a gray area in the BPT diagram in Figure 2. As Sokal et al. (2016) have already noted, Knots A and B occupy the same region as GPs in the BPT diagram. The figure further shows that both Mrk 71 and Knot A are fully consistent with the extreme GP region. For the integrated NGC 2366 system, we estimate a ratio of [OIII]/H β = 5.05 and [NII]/H α = 0.031, following the same method described in § 2.2. With these values, NGC 2366 is again quite consistent with the extreme GPs in the BPT diagram (Figure 2).

Mrk 71 and the GP starbursts therefore have similar ionization parameters U and presumably similar ionizing sources, massive stars. The average $\log(U)$ for the extreme GPs is ~ -2.5 (Stasińska et al. 2015; Jaskot & Ravindranath 2016), while James et al. (2016) estimate -1.9 ± 0.3 for Knot A. Comparing to the LBAs, Figure 2 shows that this class overlaps with average GPs in the BPT diagram, with some LBAs falling in the extreme GPs region, with line ratios [OIII] λ 5007/H β as high as \sim 5.8, and $\log[NII]\lambda 6584/H\alpha$ as low as \sim 0.04. As the figure shows, Mrk 71 is however more extreme in its ionization properties than the most extreme LBAs.

Further indication of a high ionization parameter is strong C III] λ 1907, 1909 doublet emission, often seen in low-metallicity, strongly star-forming galaxies. The C III] doublet is detected in Mrk 71 with the IUE/SWP camera (Rosa et al. 1984). From the archive spectra we

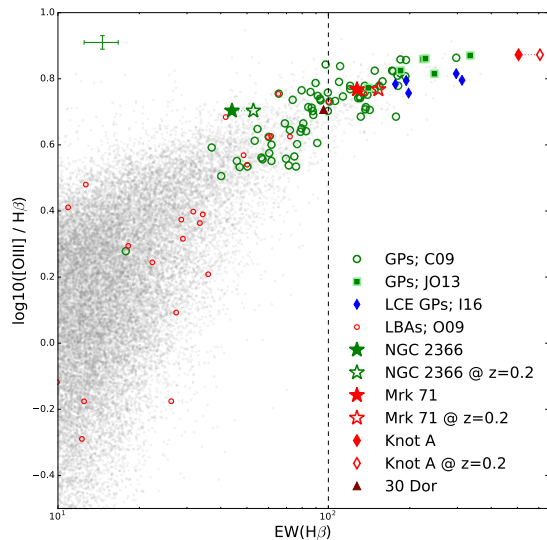


Figure 3. The observed equivalent width $EW(H\beta)$ for Mrk 71, its Knot A, and the comparison samples. Extreme GPs, with the confirmed LCE GPs among them, occupy the region with $EW(H\beta) \geq 100\text{\AA}$ defined by Izotov et al. (2011). Loci for our objects redshifted to GP distances are also shown.

obtain an equivalent width of $EW(C\text{ III}) \sim 14.5 \pm 2.0\text{\AA}$. Jaskot & Ravindranath (2016) compute photoionization models of this line with CLOUDY (Ferland et al. 1998) and investigate the predicted equivalent width of C III] with age, metallicity and ionization parameter. At the metallicity of Mrk 71, $12+\log(O/H) = 7.89 \pm 0.01$ (§ 2.5), the only model that could explain the data is the BPASS instantaneous burst model, which includes both binary interactions and effects from stellar rotation. The model predicts such a strong equivalent width only for ionization parameter $\log(U) \gtrsim -2$ and an extremely young age of 1 Myr. We note that the models do not include stars more massive than $150 M_{\odot}$, and there are indications that such may be present in Knot A (§ 2.9). Examining the CIII]-emitting region in archival *IUE* data, the C III] flux comes from an aperture that contains all of Mrk 71, including Knots A and B. Archival *HST*/*STIS* spectra of Knot B show no C III] emission. If the C III] emission is dominated by Knot A, the 1 Myr estimate above is fully consistent with several other age indicators for Knot A (§ 2.9).

GPs are selected based on their high equivalent width of $[O\text{ III}]\lambda 5007$. The average GP sample has a mean $EW([O\text{ III}]) \sim 600\text{\AA}$, with the range shown in Table 1. The equivalent width of Mrk 71 is $EW([O\text{ III}]) = 648.0 \pm 33.0\text{\AA}$ (Moustakas & Kennicutt 2006), which is consistent with this range. Note that the integrated region in the drift scan spectrum of Moustakas & Kennicutt includes both Mrk 71 and NGC 2366-II, which dilutes the measured equivalent width of Mrk 71 alone. For the integrated NGC 2366 system, we estimate the total extinction-corrected $[O\text{ III}]\lambda 5007$ flux by summing the contributions from Mrk 71+NGC 2366-II, and NGC 2363 from Moustakas & Kennicutt (2006), and the rest

of NGC 2366. For the latter we assume typical SMC $[O\text{ III}]/H\beta$ ratios, and convert to $[O\text{ III}]\lambda 5007$ flux by applying the appropriate $H\alpha$ -based weight from before (0.14) to the $H\beta$ flux. The continuum flux density is estimated from the integrated V -band flux density from Hunter et al. (2012, $V = 10.86$). The total equivalent width for the NGC 2366 system is $EW([O\text{ III}]) \gtrsim 101\text{\AA}$. Note that this is somewhat of an underestimate, since the V -band flux contains significant contributions from strong emission lines. The value range for the extreme GPs, obtained from the SDSS DR12, is $EW([O\text{ III}]) \sim 800\text{--}2000\text{\AA}$. Thus, the value for the NGC 2366 system is not within the range for the extreme GP sample, but is within that for the average GP sample (Table 1). EW measurements are sensitive to the star-formation history, and more likely to vary among objects. However, note that our estimate of the equivalent width for Knot A alone is $EW([O\text{ III}]) \sim 2200 \pm 300\text{\AA}$, based on the $[O\text{ III}]\lambda 5007$ flux reported by Izotov et al. (1997), and estimating the continuum at $\lambda 5007$ from the presented spectrum.

2.3. Specific Star Formation Rate

Both average and extreme GPs are characterized by high sSFR with ranges $s\text{SFR}(H\alpha) = 10^{-7}\text{--}10^{-9}\text{ yr}^{-1}$ by Izotov et al. (2011). They obtained the current SFR from the $H\alpha$ luminosities of the GPs, while the stellar mass estimates were derived by approximating the star formation history (SFH) by a short young burst and an older stellar population, and fitting the spectral energy distribution of each GP. While the typical GP appears as a compact object (§ 2.1), some GPs show evidence of extended underlying stellar populations. Given the distances and low surface brightness, we caution that an underlying faint extended population may not be included in current stellar mass estimates from the literature. The sSFR for the GPs therefore should be considered upper limits.

The current SFR of the host galaxy NGC 2366 is $0.13 \pm 0.03 M_{\odot}\text{ yr}^{-1}$, derived from the $H\alpha$ luminosity within a $2.6'$ aperture (Hunter et al. 2001). This value is consistent with estimates from modeling the observed color-magnitude diagram of NGC 2366 (Figure 9 in McQuinn et al. 2010). The stellar mass of NGC 2366 was reported by Lelli et al. (2014), who integrate over the SFH in McQuinn et al. and obtain a stellar mass of $26 \pm 3 \times 10^7 M_{\odot}$. For NGC 2366 one therefore obtains $s\text{SFR} = 5 \pm 1 \times 10^{-10}\text{ yr}^{-1}$. This is a factor of two lower than the lowest sSFR observed for the average GP sample. The young population in NGC 2366 is dominated by Mrk 71 (Thuan & Izotov 2005), and we estimate its stellar mass at $M_{\star} \sim 1.6 \times 10^5 M_{\odot}$ (§§ 2.9, 2.10). Stellar masses of the young population in GPs are not widely available, but note that the LCE GP in Izotov et al. (2016a) has an estimated burst stellar mass of $M_{\star} = 2.4 \pm 0.3 \times 10^8 M_{\odot}$, which is orders of magnitude larger. Our GP analog therefore samples the low-mass faint end of the GP distribution.

Table 1. Mrk 71/NGC 2366 as a GP analog

	Average GPs	Extreme GPs	NGC 2366	Mrk 71	Knot A	Knot B
$r_{1/2}$ [kpc] [optical]	$\sim 1.0^n$	0.3–2.4 ^{a,b}	2.7 ± 0.1^c
EW([OIII] λ 5007) [Å]	13–2400 ^d	800–2000 ^{a,b}	> 101	648.0 ± 33.0^e	2243 ± 345^f	435 ± 62^f
EW(H β) [Å]	9–295 ^d	100 \sim 300 ^{a,b}	~ 44.0	127.6 ± 5.5^e	505 ± 51^g	176 ± 18^g
[OIII] $\lambda\lambda$ 5007, 4959/[OII] λ 3727	0.5–14 [‡]	6 – 14 ^{a,b}	6.34	11.7 ^h	23.0 ± 0.6^i	9.4 ± 0.2^i
He II λ 4686/H β	0.0086–0.0131 ^j	0.008–0.02 ^a	$\lesssim 0.019$	0.026 ^h	$0.009 \pm 0.001^{f,h,i}$	$0.022 \pm 0.001^{i,f,h}$
[OIII] λ 5007/H β	5.18 ^j	5.7–7.3 ^{a,b}	5.10	5.86 ± 0.33^e	$7.46 \pm 0.06^{i,h}$	$6.29 \pm 0.06^{i,h}$
[NII] λ 6584/H α	0.063 ^j	0.016–0.047 ^{a,b}	0.031	0.023 ± 0.020^e	0.0119 ± 0.0004^i	0.0111 ± 0.0004^i
log(U)	–3.0 to –1.0 ^r	–2.5 ^r	...	-2.20 ± 0.39^h	-1.89 ± 0.3^h	-2.12 ± 0.23^h
T_e (OIII) [K]	$\sim 13000^k$	$\sim 13400 \sim 15500^{a,b}$...	~ 15000	$\sim 16000^{f,g,i}$	$\sim 14000^{f,g,i}$
n_e (SII) [cm ^{–3}]	$\sim 180^k$	$\sim 100 \sim 1000^{a,b}$...	~ 200	235 ± 41^i	163 ± 39^i
12 + log(O/H)	7.82–8.54 ^{k,l}	7.76–8.04 ^{a,b}	$7.89 \pm 0.01^\dagger$	$7.89 \pm 0.01^{f,m}$	$7.89 \pm 0.01^\dagger$	$7.89 \pm 0.01^\dagger$
C (H β)	0.02–0.77 ^j	0.07 – 0.16 ^{‡,b}	...	0.13 ± 0.04^h	$0.2\text{--}0.35^h$	0.2 ^{h,i}
High-velocity gas [km s ^{–1}]	FWZI $\geq 1000\text{--}1750^n$	FWZI $\sim 600^n\text{--}2460$...	FWZI $\sim 7000^o$	FWZI $\sim 7000^\dagger$	FWZI $\sim 7000^\dagger$
LIS v_{off} [km s ^{–1}]	–200 ^s	–200 ^s	-154 ± 29^t
He I λ 3819/H β	...	$\sim 0.014^a$...	~ 0.010	$\sim 0.012 \pm 0.001$	0.007 ± 0.005
Burst age [Myr]	3–5 ^k	$\lesssim 4.4^{a,b}$	$\lesssim 2^p$	3–5 ^p
sSFR(H α) [10^{-9} yr ^{–1}]	1–140 ^k	7 – 230 ^{a,b}	0.5 ^{q,c}
log(M_\star [M_\odot])	7.8–10.0 ^k	8.2–9.6 ^{a,b}	$8.41_{-0.10}^{+0.05q}$	$\gtrsim 5.2$	~ 5.1	~ 4.3

NOTE—All values are corrected for Galactic and internal reddening.

References, with apertures given for nebular data:

a - Jaskot & Oey (2013);

b - Izotov et al. (2016a,b);

c - Hunter et al. (2001);

d - Cardamone et al. (2009);

e - Moustakas & Kennicutt (2006); includes Mrk 71 and NGC 2366-II, aperture $30'' \times 90''$;

f - Izotov et al. (1997), slit width $2.0''$;

g - Sokal et al. (2016), slit width $1.3''$;

h - James et al. (2016), circular aperture of $r = 1.8''$;

i - Gonzalez-Delgado et al. (1994), slit width $1.2''$;

j - Hawley (2012);

k - Izotov et al. (2011);

l - Amorín et al. (2010);

m - Hunter & Hoffman (1999);

n - Amorín et al. (2012b);

o - Binette et al. (2009);

p - Drissen et al. (2000);

q - Lelli et al. (2014);

r - Stasińska et al. (2015), Jaskot & Ravindranath (2016);

s - Henry et al. (2015);

t - Leitherer et al. (2011);

u - McQuinn et al. (2010);

‡ - Obtained from SDSS DR12 and corrected for internal extinction assuming $C(\text{H}\beta) = 0.2$ and SMC dust law;

† - Value applies to multiple components, and is adopted from the column with references.

If we consider Mrk 71 as a dominant compact object in NGC 2366, the system is similar in morphology to LBAs (§ 2.1). Being more massive, LBAs have a slightly lower range of $\text{sSFR}(\text{H}\alpha) = 10^{-8}\text{--}10^{-10} \text{ yr}^{-1}$ (Overzier et al. 2009), which is more consistent with the value for NGC 2366.

A consequence of high sSFR is a large equivalent width of H β . In fact, Izotov et al. (2011) suggest using the observed H β equivalent width of $\geq 100\text{Å}$ as a selection

criterion for GP-like galaxies with strong star formation. We show EW(H β) for the GP and LBA samples in Figure 3, and note that the Izotov et al. criterion of observed $\text{EW} \geq 100\text{Å}$ includes about half of the average GP sample and the full sample of extreme GPs, while the only LBA which makes the cut is also a GP. For the average GPs, the range in EW(H β) in Table 1 is obtained from the SDSS DR12. For the extreme GPs, the range of EW(H β) is 100 to $\sim 300\text{Å}$ (Izotov et al.

2011). In Figure 3 and Table 1 we show our estimate of the equivalent width of $H\beta$ for the host galaxy NGC 2366. We obtain this value by assuming the total $H\beta$ luminosity is 2.86 times less than the total $H\alpha$ luminosity for NGC 2366 ($L(H\alpha) = 1.3 \times 10^{40}$ erg s^{-1} ; Kennicutt et al. 2008), using a distance of 3.4 Mpc, and estimating the continuum emission from the integrated B -band flux density in Hunter et al. (2001, $B = 11.15$). The $EW(H\beta) \sim 44.0 \text{ \AA}$ for NGC 2366, which is consistent with average GPs values.

Drift-scan spectra of Mrk 71 from Moustakas & Kennicutt (2006), yield $EW(H\beta) = 127.6 \pm 5.5 \text{ \AA}$. These data include a contribution from NGC 2366-II, as discussed in Sec. 2.2. For Knot A, which is responsible for most of the similarities between Mrk 71 and GPs, $EW(H\beta) = 505 \pm 51 \text{ \AA}$ within a $1.3''$ aperture (Sokal et al. 2016). When isolated, it thus has a more extreme equivalent width than even the extreme GPs, as shown in Figure 3.

2.4. T_e and n_e

In extreme GPs the $[OIII]\lambda\lambda 5007, 4959/\lambda 4363$ ratio indicates electron temperatures $T_e \sim 15000$ K, while from $[SII]\lambda 6716/\lambda 6731$ one obtains electron densities $n_e = 100\text{--}1000 \text{ cm}^{-3}$ (Jaskot & Oey 2013). The electron temperature has been measured in the nebular emission from Knot A by several authors (Gonzalez-Delgado et al. 1994; Izotov et al. 1997; Sokal et al. 2016) and is on average ~ 16000 K. Gonzalez-Delgado et al. (1994) also measure the electron density of the Knot A to be $n_e = 235 \pm 41 \text{ cm}^{-3}$. We note that most of the nebular measurements are generally based on apertures on the order of $1''$ and are therefore characteristic of the SSC environment, rather than conditions within Knot A itself. The reported values are consistent with electron temperatures and electron densities seen in the extreme GP sample (Table 1.)

2.5. Abundances

Average GPs have sub-solar abundances with a range $12 + \log(O/H) \sim 7.8 - 8.5$, based on the so-called “direct” method, which uses the electron temperature derived as above, from the $[O III] \lambda\lambda 4959, 5007/\lambda 4363$ ratio to obtain the oxygen abundance of the ionized gas from the collisionally excited lines of $[OIII]$ and $[OII]$ (e.g., Amorín et al. 2010; Izotov et al. 2011). The extreme GPs have a range spanning lower abundances, $12 + \log(O/H) = 7.8 - 8.0$ (Izotov et al. 2011; Izotov et al. 2016a,b). The abundance of Mrk 71 as measured from Knot A is $12 + \log(O/H) = 7.89 \pm 0.01$, using the same method (Izotov et al. 1997), and is thus consistent with both average and extreme GPs.

Another method for obtaining abundances uses optical recombination lines like $O II \lambda 4649$. Although these lines are often too weak to be detected, the derived abundances are much more robust, and almost independent of temperature. Using recombination lines to obtain the oxygen abundance for Mrk 71, Esteban et al.

(2002) find a higher value of $12 + \log(O/H) = 8.19 \pm 0.11$. This is in good agreement with Luridiana et al. (1999) who are only able to reconcile the observed emission-line spectrum of Mrk 71 with photoionization models when using a higher abundance of $12 + \log(O/H) = 8.2$. This higher abundance for Mrk 71 would imply more dust, which is to the detriment of LyC escape since dust readily attenuates ionizing radiation. However, the confirmed LBA LyC-leaker found by Borthakur et al. (2014) has an abundance of $12 + \log(O/H) = 8.67$, which is much higher than the abundance in Mrk 71. Similarly high abundances are found for all three LBAs which are LCE candidates in Heckman et al. (2011). We caution that the LBA abundances were estimated using the semi-empirical “O3N2” method from Pettini & Pagel (2004), but even if there is a systematic overestimate, the obtained values suggest that the LBA abundances are in any case higher than for GPs.

We stress that, regardless, the abundance of Mrk 71 is fully consistent with those of both average and extreme GPs when consistently determined using the same “direct” method, as described above.

2.6. Reddening and Dust

The average GPs have a low extinction correction factor $C(H\beta)$ ranging between 0.02–0.77 (Hawley 2012), with the extreme LCE GPs on the lower end of this distribution with values 0.07–0.13 (Izotov et al. 2016a,b). For the extreme GPs in Jaskot & Oey (2013) we measure $C(H\beta) \leq 0.16$ from SDSS spectra, and this is the maximum value we present in Table 1 for the combined extreme GP sample. The average $C(H\beta)$ in Mrk 71 is $\sim 0.13 \pm 0.04$ (James et al. 2016), consistent even with the extreme GP sample. The low average $C(H\beta)$ factor implies a low dust content.

The presence of dust can also be inferred from emission in the IR regime. Izotov et al. (2011, 2014) study the IR emission from hot dust of a sample of compact star-forming $z < 0.6$ galaxies using data from WISE. Among these are 16 GPs from the average GP sample. The $3.4\mu\text{m} - 4.6\mu\text{m}$ and $4.6\mu\text{m} - 22.0\mu\text{m}$ colors are a proxy of the slope of the spectrum at these wavelengths. For the GPs the observed average colors are 1.9 and 7.3, respectively, indicating the presence of hot dust. However, we stress that these GPs are not representative of the average GP sample since they were selected on the basis of having very red WISE colors.

To compare to NGC 2366, we use the spatially integrated IR values available as part of the Spitzer Local Volume Legacy survey in IRAC and MIPS bands (Dale et al. 2009). To cover the same wavelength range we use IRAC1 ($3.6\mu\text{m}$), IRAC2 ($4.5\mu\text{m}$), and MIPS1 ($24\mu\text{m}$), and obtain $3.6\mu\text{m} - 4.5\mu\text{m} = -0.3 \pm 0.2$, and $4.5\mu\text{m} - 24\mu\text{m} = 0.3 \pm 0.2$. These colors are typical of the star-forming galaxies in Dale et al. (2009). While the filters are slightly different, it cannot account for the large differences with the WISE observations. Due to the selection effect of the WISE GPs we can only conclude

that there exist GPs which have much steeper slopes over the wavelength range $3.6\mu\text{m}$ – $24\mu\text{m}$, and therefore likely more dust than NGC 2366.

2.7. Column density of neutral gas

Resonant UV absorption lines produced in the neutral interstellar medium (ISM) of star-forming galaxies are sensitive to its opacity and covering factor (e.g. Heckman et al. 2001, 2011; Leitherer et al. 2011). In LBAs, Heckman et al. (2011) use the low equivalent widths of interstellar C II $\lambda 1335$ and Si II $\lambda 1260$ absorption lines to infer significant leakage of LyC from three out of eight LBAs in their sample. In extreme GPs the non-detection of these absorption lines has been suggested as an indication of very low column density of the intervening gas, increasing the likelihood of LyC leakage from these objects (Jaskot & Oey 2014).

Even if such absorption is detected one may still be in the linear part of the curve of growth, where the column density is low. Using HST/FOS and GHRS observations of local starbursting galaxies, Leitherer et al. (2011), show that the equivalent widths of several low-ionization state, UV absorption lines (LIS) like Si II $\lambda 1260$, OI–Si II $\lambda 1303$, Si II $\lambda 1526$, and C II $\lambda 1335$ for Mrk 71 are among the weakest in their sample of local starburst galaxies, while Fe II at $\lambda 1608$, $\lambda 2370$, $\lambda 2600$, and Mg II $\lambda 2800$ are not even detected. This suggests that the line of sight towards Mrk 71 may be optically thin, although this could also be due to its low metallicity. However, we note that significant absorption in these lines is detected in I Zw 18 and SBS 0335–052 (James et al. 2014), which have metallicities much lower than that of Mrk 71.

Using the ratio of Si II $\lambda 1260/\lambda 1526$, Leitherer et al. (2011) demonstrate that most of their sample of local starburst galaxies is optically thick in Si II, with $\lambda 1260/\lambda 1526 \sim 0.5$ – 2 . However, for Knot A in Mrk 71, their data show that the corresponding ratio is $\lambda 1260/\lambda 1526 = 6.0 \pm 0.3$ (Leitherer et al. 2011, their Table 8), where optically thin values correspond to a ratio of ~ 5.2 . Thus, the Si II transitions are optically thin, implying similar conditions for H I.

Under optically thin conditions, we can obtain the column density of Si II from the equivalent width of, e.g., the Si II $\lambda 1260$ line, from which we obtain $N(\text{Si II}) = 2 \times 10^{14} \text{ cm}^{-2}$. To translate this to H I column density one would need the Si II abundance, which in turn depends on the total Si abundance and the Si ionization structure inside of the cloud. Modeling the latter is beyond the scope of this paper, and so we provide only a coarse upper limit by approximating that H I coexists exactly with Si II. The total silicon abundance for Mrk 71 is $12 + \log(\text{Si}/\text{H}) = 6.3$ (Garnett et al. 1995), giving an upper limit on the H I column density of $N(\text{H I}) \lesssim 10^{20.0} \text{ cm}^{-2}$. While consistent with optically thin Si II transitions, this upper limit is too coarse to definitively demonstrate optically thin conditions for H I, which occur for $N(\text{H I}) \lesssim 10^{17.2} \text{ cm}^{-2}$.

Another good tracer of neutral, diffuse gas is absorp-

tion in the resonance doublet Na I $\lambda\lambda 5890, 5896$ in the optical. In Mrk 71, Schwartz & Martin (2004) do not detect Na I in absorption and put upper limits on the column density of Na I at $< 0.57 \times 10^{12} \text{ cm}^{-2}$. They suggest this to be indicative of a lack of neutral gas in the line of sight, and significant leakage of ionizing radiation from this galaxy. Similarly to Si II, we can apply the same method to estimate an H I column density from the upper limit on the Na I doublet. Taking the SMC abundances as representative of Mrk 71 (§2.5), $\log(\text{Na}/\text{H}) \sim -8.50$ (Cox et al. 2007). Approximating that H I coexists exactly with Na I, the upper limit on the Na I non-detection implies an H I column density of $N(\text{H I}) \lesssim 10^{20.5} \text{ cm}^{-2}$. This upper limit is again not a sufficient condition for LyC escape. Taking the abundance of Na I to be equal with that of total Na is even less likely to be a good approximation here since the first ionization potential of Na is only 5.1 eV, and thus much of the Na could be ionized in an otherwise neutral hydrogen cloud. But in any case, the non-detection in absorption of Na I and other low-ionization species, as well as the optically thin Si II transitions, are consistent with LyC leakage from Mrk 71.

2.8. Kinematics

Amorín et al. (2012b) select five GPs from the Cardamone et al. (2009) sample for high-resolution follow-up spectroscopic observations, and detect broad H α wings of full width zero intensity FWZI $> 1000 \text{ km s}^{-1}$ in all of them. We note that one of these objects, SDSS J004054.31+153409.8, falls into the extreme GP region in Figure 2 with $\log([\text{OIII}]/\text{H}\beta) = 0.8$ and $\log([\text{NII}]/\text{H}\alpha) = -1.4$, while the other four have more typical excitation, with average $\log([\text{OIII}]/\text{H}\beta) = 0.6$ and $\log([\text{NII}]/\text{H}\alpha) = -1.0$. For the extreme GPs in Jaskot & Oey (2013), we measure a range of FWZI = 770–2460 km s^{-1} . Since the broad wings are found in both the average and the extreme GP samples, the kinematics may have similar origin. Amorín et al. interpret these features as rapid outflows of ionized gas due to strong stellar winds from massive stars in combination with expansion of multiple supernova remnants. At the redshift of these GPs, $z \sim 0.2$, their unresolved appearance prohibits any detailed testing of this scenario. However, similarly broad features are present in Mrk 71, which might provide clues to their origin in GPs. In Mrk 71 a faint, broad spectral component of full width half maximum FWHM $\sim 2400 \text{ km s}^{-1}$ (FWZI $\sim 7000 \text{ km s}^{-1}$) in H α and [O III] $\lambda 5007$ was detected by Roy et al. (1992) and Gonzalez-Delgado et al. (1994) over most of the complex. These authors found that conventional mechanical feedback from stellar winds and supernovae are unlikely to explain the high velocities. Recently, Binette et al. (2009) showed that the observations can be reproduced by turbulent mixing layers, in which the broad wings result from acceleration of photoionized turbulent gas entrained from dense clumps by a strongly supersonic SSC wind.

Outflows of interstellar gas accelerated by massive stellar winds and supernovae can be traced by UV absorption lines that are blueshifted with respect to the systemic velocity. Such blueshifting is detected in, for example, the C II $\lambda 1335$ and Si III $\lambda 1206$ lines in LBAs, implying strong outflow velocities of gas reaching ~ 1500 km s $^{-1}$ (Heckman et al. 2011). We caution that in the case of LCE LBAs the outflow may be AGN-assisted since these galaxies are found in the SF-AGN composite region in the BPT diagram; however no evidence of any AGN has been found (Overzier et al. 2009). Jaskot & Oey (2014) and Henry et al. (2015) find broad and blueshifted Si II $\lambda 1260$ and C II $\lambda 1335$ absorption lines for two extreme GPs, indicative of outflow of cool neutral gas. Leitherer et al. (2011) observe these latter two lines in Mrk 71, which also appear offset from photospheric features for Knot B. The velocity offsets v_{off} are on the order of 200 km s $^{-1}$ in both GPs and Mrk 71, as shown in Table 1. We caution that the value for Knot A published by Leitherer et al. (2011) is unreliable since there are no known photospheric lines observed in this object, to serve as the systemic reference (Drissen et al. 2000).

2.9. Stellar population of Knot A

Knot A hosts a massive, enshrouded SSC. As mentioned earlier, no stellar features have ever been confirmed in this object, and so we rely on indirect inference of its stellar properties. Using a total H α luminosity for Mrk 71 of $L(\text{H}\alpha) = 1.4 \times 10^{40}$ erg s $^{-1}$, which is dominated by Knot A (§ 2), Gonzalez-Delgado et al. (1994) estimate a lower limit to the total stellar mass of $M_{\star} \gtrsim 3.4 \times 10^5 M_{\odot}$. This value differs by a factor of ~ 6 from the estimate of $M_{\star} = 5.3 \times 10^4 M_{\odot}$ for Knots A and B combined, by Sokal et al. (2016), who instead normalize by the V band luminosity. This difference in stellar mass estimates can likely be reconciled by considering the extinction. Sokal et al. assume an extinction $A_V = 0.0$ for Knot A, which is an underestimate since the SSC is still enshrouded in its natal cloud (§2). While much of the literature reports $C(\text{H}\beta) \approx 0.2$ for Knot A, this is usually obtained from ground-based apertures on the order of 1", and it is clear from the $C(\text{H}\beta)$ map from James et al. (2016), which is based on new high-resolution HST data, that a lower limit to the extinction correction is $C(\text{H}\beta) \gtrsim 0.35$ for the dense knot itself. A factor of 6 increase to the V band flux requires $A_V = 1.9$, which translates to $C(\text{H}\beta) = 0.68$ using the Calzetti et al. (2000, $R_V = 4.1$) dust attenuation law. A comparable extinction of $A_V \geq 1.5$ is typical among very young clusters with ages ≤ 3 Myr (Whitmore & Zhang 2002). There are also additional differences between the methods used to obtain the mass estimates. Gonzalez-Delgado et al. (1994) use solar metallicity evolutionary models and mass loss prescription, and an assumed age of 3–5 Myr; while Sokal et al. (2016) use low-metallicity, high-mass loss models. Accounting for these differences in inputs can further help to reconcile the two mass es-

timates.

We perform our own estimate of the stellar mass for Knot A by scaling with the revised H α luminosity measurement for Mrk 71 by James et al. (2016), $L(\text{H}\alpha) = 8.4 \times 10^{39}$ erg s $^{-1}$. We use a “standard” STARBURST99 model (v7.0; Leitherer et al. 2014), adopting a Kroupa IMF, instantaneous starburst, and $Z = 0.2Z_{\odot}$. We assume that Knot A has an age of 1 Myr and H α luminosity that is 90% that of Mrk 71 (§2). The resulting stellar mass of Knot A is $\sim 1.3\text{--}1.4 \times 10^5 M_{\odot}$, depending on whether we use tracks without or with rotation, respectively. This is our adopted stellar mass for Knot A that we list in Table 1.

The high ionization parameters in extreme GPs, $\log(U) = -2.5$, suggest very young ages. Stellar population synthesis models, together with photoionization models, suggest an upper age limit of $\lesssim 4$ Myr (Jaskot & Oey 2013). Knot A in Mrk 71 has a comparable ionization parameter $\log(U) = -1.89 \pm 0.3$ (James et al. 2016) and excitation as the GPs (Figure 2), and therefore could be similar in age. The GP ages are consistent with a paradigm in which mechanical feedback has enough time to facilitate LyC escape by punching holes in the ISM, while hot, massive stars of ages 3–5 Myr, dominated by WR stars, produce the escaping ionizing photons (e.g., Fernandez & Shull 2011; Zastrow et al. 2013).

There are indications, however, of an even younger age for Knot A, which could mean a possible shift in this paradigm. Here again, the properties of Knot A bear strong resemblance to those of extreme GPs. In particular, the presence of nebular He I $\lambda 3819$ is readily detected in the extreme GPs (Jaskot & Oey 2013), with average He I $\lambda 3819/\text{H}\beta = 0.014 \pm 0.006$ and $\text{EW}(\text{He I } \lambda 3819) = 1.95 \text{ \AA}$. The He I $\lambda 3819$ line is also clearly detected in Knot A, as seen in the spectrum of Sokal et al. (2016). Applying the extinction correction for Knot A, $C(\text{H}\beta) \gtrsim 0.35$ (§ 2.6), we measure a line ratio and equivalent width in this spectrum similar to GPs: He I $\lambda 3819/\text{H}\beta = 0.012 \pm 0.001$ and $\text{EW}(\text{He I } \lambda 3819) = 1.9 \pm 0.3 \text{ \AA}$. Using evolutionary synthesis models, González Delgado et al. (1999) show that this line is strongest at ages 0–2 Myr, when $\text{EW}(\text{He I } \lambda 3819) = 2.6\text{--}1.5 \text{ \AA}$, respectively, and significantly weakens or disappears at ≥ 3 Myr since it becomes dominated by stellar absorption. Since Knot A is dominated by nebular emission and no stellar features are visible, the interpretation of this nebular line is more ambiguous. However, its presence suggests that both the extreme GPs and the starburst in Knot A are of similarly young age $\lesssim 2$ Myr. This is consistent with an age estimate for Knot A of $\lesssim 1$ Myr by Drissen et al. (2000), based on the still strongly embedded condition of the young super star cluster, also stressed by Sokal et al. (2016).

Another indication of Knot A’s very young age is the lack of classical WR stars (Drissen et al. 2000), which appear at ages around 3 Myr. They can be identified by a broad “blue bump” in the continuum near $\lambda 4650$, due

to N III $\lambda\lambda 4634\text{--}4641$ and He II $\lambda 4686$ emission associated with WN stars, indicating an age of $\sim 3\text{--}5$ Myr. While there is narrow, nebular He II $\lambda 4686$ emission clearly detected in the Binette et al. (2009) echelle spectrum of Knot A in Mrk 71, there also seems to be a very faint, broad bump centered only at $\lambda 4686$. Although those authors attribute this faint feature to turbulent mixing layers, it could also be a faint detection of WN features from very massive stars (VMS, e.g., Crowther et al. 2010; Crowther & Walborn 2011; Gräfener & Vink 2015; Smith et al. 2016). VMS are $150\text{--}300 M_{\odot}$ O-type supergiants, which have short lifetimes of $1\text{--}3$ Myr and are found in high-mass ($\gtrsim 10^4 M_{\odot}$), extremely young clusters (e.g. Crowther et al. 2010). The VMS are of class O2–3.5 If* at the zero age main sequence, and within the first $1\text{--}2$ Myr of their lives become “slash” stars of class O2–O3.5 If*/WN5–7, with WR features in their spectra (Crowther & Walborn 2011). Such VMS stars of initial masses up to $320 M_{\odot}$ have been identified in R136 in the 30 Doradus star-forming region of the Large Magellanic Cloud (Crowther et al. 2010). Additionally, Smith et al. (2016) show that in cluster #5 in NGC 5253, the broad He II $\lambda 4686$ emission likely arises from stellar emission of VMS with $\geq 100 M_{\odot}$ and ages of $1\text{--}2$ Myr. The presence of VMS stars in Knot A has already been suggested by James et al. (2016) to account for the extreme stellar temperatures required to ionize He II. If the faint, broad He II emission in Knot A is real, it could further support the presence of VMS stars, which would be consistent with its implied age of $\lesssim 2$ Myr.

On a final note, we again consider the detection of the C III] $\lambda 1909$ doublet in Mrk 71. As discussed in §2.2, the only model prediction of Jaskot & Ravindranath (2016) that could explain the observed C III] EW = $14.5 \pm 2.0 \text{ \AA}$ in Mrk 71 is the one with an age of 1 Myr. The observed equivalent width appears to rule out models for ages ≥ 3 Myr, implying that this emission is more likely to come from Knot A, since Knot B has a well established age of $3\text{--}5$ Myr, based on its observed stellar population (§2.10).

2.10. Knot B

In the above comparisons, we have concentrated on the properties of Knot A, since it strongly dominates the ionizing luminosity and excitation of Mrk 71 (e.g., Gonzalez-Delgado et al. 1994; Drissen et al. 2000). However, while not as extreme in its properties, the exposed cluster, Knot B, also contributes to the GP-like properties of the complex.

Knot B is a lower-mass SSC with stellar mass $1.2 \times 10^4 M_{\odot}$ reported by Sokal et al. (2016). We obtain a similar mass of $1.5 \times 10^4 M_{\odot}$ with the same STARBURST99 model as for Knot A, but assuming an age of 3 Myr and only 11% of the Mrk 71 $L(\text{H}\alpha)$ (§ 2). Knot B’s stellar population has been spectroscopically studied with ground-based observations from the William Herschel Telescope by Gonzalez-Delgado et al. (1994)

and *HST*/FOS observations by Drissen et al. (2000). Gonzalez-Delgado et al. (1994) detect P-Cygni, stellar wind signatures from C IV $\lambda 1550$ and N V $\lambda 1240$ doublets, as well as WR features consisting of both a blue bump at $\lambda 4660$ and a red bump at $\lambda 5800 \text{ \AA}$, indicating the presence of WC stars. Drissen et al. (2000) perform UV spectral synthesis of Knot B and conclude that around 800 B and 40 O stars must be present, which can account for only $\sim 11\%$ of the total number of photons needed to ionize Mrk 71 (§2). Through *HST* narrow-band imaging and long-slit spectroscopy, the existence of broad WR features in emission at 4660 \AA and 5810 \AA has been well established, as well as a strong, narrow He II $\lambda 4686$ line of nebular origin (Drissen et al. 1993; Gonzalez-Delgado et al. 1994; Drissen et al. 2000). There are three known WR stars in the core of Knot B, with their global spectrum dominated by an early-type WC4 star as indicated by the $\lambda 4650/5810$ ratio (Drissen et al. 2000). Sokal et al. (2016) suggest that as many as 8 WR stars are present. The presence of these classical WR stars sets the age of Knot B at $3\text{--}5$ Myr.

The excitation for the region around Knot B is high, as traced by the [OIII]/[OII] ratio of $\sim 9.4 \pm 0.2$ (Gonzalez-Delgado et al. 1994). The implied ionization parameter is also high, as found by James et al. (2016), who obtain $\log U = -2.12 \pm 0.23$. This is consistent with both excitation dominated by WR stars and the likely presence of significant Knot A contribution. Gonzalez-Delgado et al. (1994) find an electron temperature and density in Knot B similar to those in Knot A, namely, $T_e \sim 14000 \text{ K}$, and $n_e = 163 \pm 39$.

In contrast to Knot A, where the Si II $\lambda 1260/\lambda 1526$ ratio is optically thin (see §2.8), in the line of sight to Knot B, the value of $\lambda 1260/\lambda 1526 = 0.4$ (Leitherer et al. 2011), and thus suggests an optically thick line of sight. Information about Knot B is included in Table 1.

As seen in Figures 1 and 4, Knot B appears to have generated a superbubble with strong shell morphology to the east, and a blow-out region to the north. This is consistent with the substantial mechanical feedback generated by a massive, somewhat evolved super star cluster. Fabry-Perot observations by Roy et al. (1991) confirm that the shell is expanding, with line splitting in $\text{H}\alpha$ and [OIII] showing expansion velocities of $\sim 20 \text{ km s}^{-1}$. These kinematics are seen in a region centered on the blowout, which, as seen in Figure 5, extends over a 200-pc region to the north and coincides with a low-density chimney seen in VLA HI line observations of NGC 2366 in the LITTLE THINGS survey (e.g., Walter et al. 2008; Hunter et al. 2012). The blowout subtends a projected angle of $\sim 30^\circ$, which corresponds to a solid angle of 2% out of 4π steradians, assuming axisymmetric geometry. This may be an upper limit due to projection effects. X-ray emission from the blowout is marginally detected in *XMM-Newton* observations by Thuan et al. (2014), as expected from mechanical feedback.

As discussed in Section 2.8, outflows have been detected in both GPs and LBAs, and are likely to be ac-

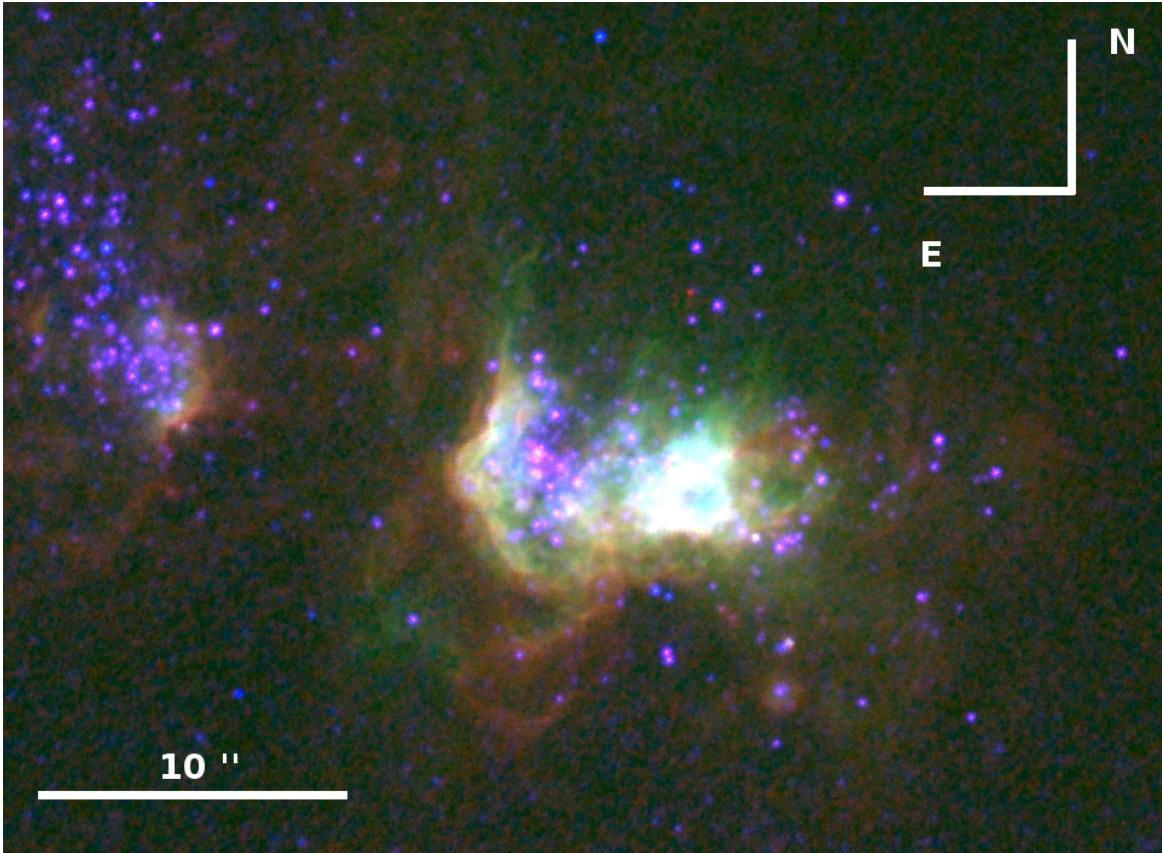


Figure 4. Three-color image of Mrk 71, in F373N ([O II] λ 3727; red), F502N ([O III] λ 5007; green), and F469N (He II λ 4686; blue), showing the highly ionized [O III]-dominated region extending to the north from Mrk 71.

accompanied by low column densities. While the observed velocities seen in GPs and LBAs are much higher, we note that the blowout seen here appears to be largely transverse to the line of sight, minimizing the observed kinematics. It is likely that mechanical feedback from Knot B cleared large areas in Mrk 71, reducing the optical depth for Knot A as well. We discuss this further in §3.

3. NGC 2366 AS LCE CANDIDATE

We have established above that the properties of NGC 2366, and Mrk 71, driven by Knot A in particular, are quantitatively consistent with GPs and spectroscopically confirmed LCE GPs, in terms of morphology, excitation, sSFR, abundances, dust reddening, neutral gas column density and gas kinematics. We now further examine the likelihood that NGC 2366 is an LCE.

Ionization-parameter mapping (IPM, Pellegrini et al. 2012) can help diagnose density-bounded, optically thin nebulae using spatially resolved emission-line data. In Figure 4 we use [O II] λ 3727, [O III] λ 5007, and He II λ 4686 as the red, green, and blue channels, respectively, of the 3-color image. Figure 4 shows that the central, highly ionized region ([O III]; green) is bounded by lower-ionization zones in all directions except to the north, where we see unbounded strong emission in [O III] in the direction of the blowout described above (Fig-

ure 5). In all other directions, a transition zone to lower ionization ([O II]; red) and neutral gas is visible in Figure 4. This implies that the region is probably optically thin in the LyC, along the blowout. The nebular morphology also strongly suggests that the optically thin region corresponds to an ionized outflow. The ionization structure and morphology is consistent with the extreme nebular excitation and ionization parameter implied by the [O III]/[O II] ratio and presence of He II λ 4686 (§ 2.2). As discussed in § 2.9, VMS stars may be responsible for these properties.

The detection of C III] λ 1909 emission in Mrk 71 may also indicate conditions favorable to LyC escape. Both observations (Stark et al. 2014) and models (Jaskot & Ravindranath 2016) show that galaxies with strong C III] have high ionization parameters, low metallicities and young stellar populations. Jaskot & Ravindranath (2016) suggest that C III] λ 1909 emission that is lower than predicted for a given age and metallicity might indicate LyC escape. These authors estimate that a decrease in the strength of C III] of 2–68% could imply up to 20% escape of LyC photons. If taken at face value, the equivalent width we estimate from the available data, $EW(C\ III]) = 14.5 \pm 2.0 \text{ \AA}$, is lower than the predicted model value by $\sim 12\%$, which would be consistent with LyC escape. Within the uncertainty, however, the data are also marginally consistent with the expected value

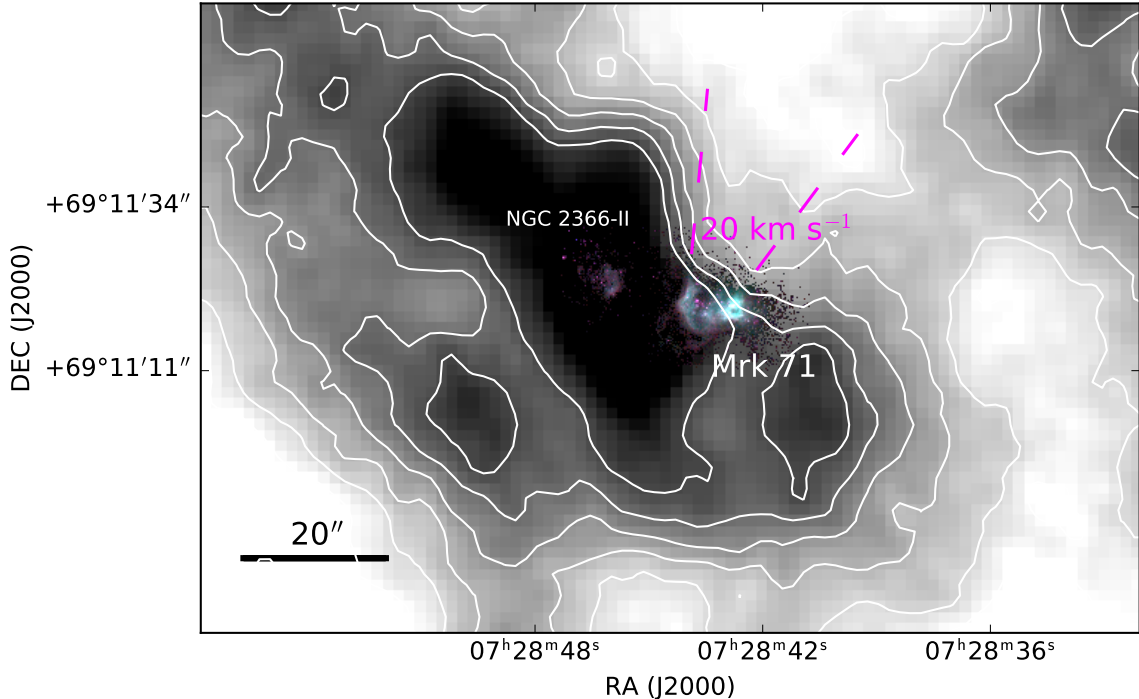


Figure 5. Mrk 71 three-color image superimposed on a gray scale, integrated $N(\text{H I})$ map of the NGC 2366 system (Walter et al. 2008). The H I map has major and minor axes of the synthesized beam of $13.1''$ and $11.85''$, respectively, a channel width of $\Delta v = 2.6$ km/s, and a total bandwidth of 1.56 MHz. Overplotted are H I column density contours between $1\text{--}5 \times 10^{21} \text{ cm}^{-2}$, in bins of 0.5. The location of the 20 km s^{-1} blowout region from Roy et al. (1991) is also indicated. The RGB bands are the same as in Figure 4.

from a $\log U = -2$ model. We note that another strong local C III] emitter is Tol 1214–277, which has an equivalent width similar to Mrk 71 (Rigby et al. 2015), and is suspected of leaking LyC based on analysis of its peculiar Ly α profile (Verhamme et al. 2015).

While Figure 5 shows detection of H I toward Mrk 71, it is likely that clumping of this gas in the foreground may also allow for an optically thin line of sight. In a “picket fence” model (Heckman et al. 2001; Bergvall et al. 2006), an optically thick H I medium with covering fraction less than unity allows LyC photons to escape unimpeded through low density channels. It also seems likely that most of the detected H I is located behind Mrk 71. As described in §2.7, low absorption columns for Knot A are suggested by the optically thin Si II $\lambda 1260/\lambda 1526$ ratio and weak detections or non-detections of other low-ionization and neutral species. The low reddening (§ 2.6) is further consistent with these conditions, facilitating the escape of LyC emission.

Thus, we conclude that NGC 2366, and in particular Mrk 71, is an excellent candidate for LyC emission and could provide important clues to the conditions and processes for the escape of ionizing radiation in GPs and higher-redshift galaxies. The wealth of spatially resolved data for Mrk 71 show a major, two-stage starburst, probably triggered by the interaction between NGC 2366 and NGC 2363. The Knot B SSC was formed 3–5 Myr ago, generating a superbubble and blowout from the plane of

the host galaxy. The Knot A SSC formed nearby, $\lesssim 1$ Myr ago, and while still enshrouded, its powerful luminosity drives the high ionization parameter and other extreme excitation properties of the Mrk 71 complex. The synergy between the feedback from the older Knot B and the younger Knot A may be one recipe for enabling LyC escape from this galaxy; similar two-stage starbursts are seen in other SSC systems, for example, the dual system of R136 and Hodge 301 in 30 Dor (e.g., Sabbi et al. 2016). The similarity to the integrated properties of GPs suggest that such processes may also be important in those objects and other LCE candidates. We will report a more detailed analysis of the physical processes in Mrk 71 in a forthcoming work.

3.1. A faint local population of LCEs?

We noted earlier that an important difference between NGC 2366 and the GPs is that the former is much fainter than average, and its young stellar population is much less massive (§ 2). Coincidentally, the cosmic star-formation rate density decreases by a factor of ~ 0.5 between $z = 0.2\text{--}0.4$ and the present (e.g. Madau & Dickinson 2014), which is about the same as the difference in sSFR between the GPs and Mrk 71/NGC 2366.

The system is 1–2 orders of magnitude fainter in FUV than typically observed for the average GPs sample. Therefore, NGC 2366 probes an unexplored region in the GP mass and luminosity function. The detection of a GP analog and LCE candidate at a distance of only

3.4 Mpc argues against the rarity of faint GP-like objects, and thus faint LCE candidates may be common. Objects with similar properties to NGC 2366, and in particular Mrk 71, could be numerous at higher redshifts but remain undetected. Indeed, it would take high magnification for such objects to be detected at high redshift, as recently done by [Vanzella et al. \(2017\)](#), who identify two lensed low-mass ($< 10^7 M_\odot$), low-metallicity (1/10 solar) compact objects at $z = 3.2$, showing optical oxygen line ratios consistent with extreme GPs. If such objects indeed translate into a substantial LCE population, it would be consistent with the growing evidence that extremely faint galaxies contribute critically to the reionization of the Universe (e.g. [Razoumov & Sommer-Larsen 2010](#); [Alvarez et al. 2012](#); [Bouwens et al. 2015](#); [Atek et al. 2015](#); [Stark 2016](#); [Dijkstra et al. 2016](#)). In general, these works suggest that low-luminosity LCEs should have higher LyC escape fractions. Our crude estimate of the blowout opening angle in § 2.10 suggests, at face value, a LyC escape fraction from NGC 2366 of $\lesssim 2\%$, which is similar to values seen in other confirmed local LCEs. However, as discussed above, the LIS absorption lines hint that the optical depth in the line of sight may also be low, suggesting the possible existence of multiple channels for the escape of ionizing photons. We suggest that NGC 2366 may be representative of such a population of faint LCE galaxies at high redshift. As such, it offers a unique opportunity to investigate in detail the properties of such objects and mechanisms for LyC escape.

4. CONCLUSION

We have presented a comprehensive, quantitative comparison of the properties of NGC 2366 and its giant H II region, Mrk 71, with Green Pea galaxies, and find that they are in remarkable agreement. As summarized in Table 1, NGC 2366, dominated by Mrk 71, is quantitatively similar to GPs in almost all its properties, including very high excitation, strong EW([OIII]) $\sim 2200 \pm 300$ Å, extreme line ratios of [OIII] $\lambda\lambda 5007, 4959$ /[OII] $\lambda 3727 \sim 17$, nebular $T_e \sim 15,000$ K and $n_e \sim 200$ cm $^{-3}$. Like in the GPs, the resulting high ionization parameter of $\log U \sim -2.2$ is generated primarily by an extremely young burst, perhaps $\lesssim 1$ Myr old, corresponding to a high sSFR $\sim 5 \times 10^{-10}$ yr $^{-1}$ and compact morphology. Other similar properties include high-velocity gas kinematics (FWHM ~ 2400 km s $^{-1}$) and Doppler shifts indicative of outflow, low reddening ($C(H\beta) \sim 0.13$), and low implied neutral gas absorption columns. Thus NGC 2366 is an outstanding GP analog.

The GP class is known for offering strong LCE candidates, some of which are spectroscopically con-

firmed. Indeed, we also find compelling evidence of possible LyC escape from our newly identified GP analog, Mrk 71/NGC 2366. The wealth of existing data for this system, including HST nebular imaging (e.g., [James et al. 2016](#)), spatially resolved, nebular kinematic data (e.g., [Roy et al. 1991](#)), and H I mapping (e.g., [Hunter et al. 2012](#)) show a clear blowout and outflow to the north, generated by the older of Mrk 71’s two super star clusters, Knot B. Ionization-parameter mapping indicates that this blowout region is optically thin, with the ionization dominated by the extremely young, still enshrouded super star cluster, Knot A, whose ionizing luminosity is an order of magnitude greater than that of Knot B. Knot A is a remarkable object, with strong similarities to R136 in 30 Dor and NGC 5253 #5, and it may contain VMS stars. This object may also be optically thin to the LyC in our line of sight, as suggested by weak detection or non-detection of low-ionization species in absorption, for example, C II $\lambda 1335$, Fe II $\lambda 1608, \lambda 2370, \lambda 2600$, Mg II 2800 ([Leitherer et al. 2011](#)), and Na I $\lambda\lambda 5890, 5896$ ([Schwartz & Martin 2004](#)). Si II is optically thin, as indicated by the ratio of Si II $\lambda 1260$ / Si II $\lambda 1526$ ([Leitherer et al. 2011](#)). The C III $\lambda 1909$ emission also may be lower than expected, and suggestive of optically thin conditions ([Jaskot & Ravindranath 2016](#)). These species all suggest low neutral column densities, consistent with the likelihood of LyC escape, and consistent with similar observations of GP LCE candidates. Also similar to GPs, observed low dust reddening in Mrk 71 and extreme excitation conditions further favor the escape of LyC radiation.

Mrk 71 is however two orders of magnitude less luminous than average and extreme GPs. The mass ($2.6 \times 10^8 M_\odot$) and metallicity ($12 + \log(O/H) = 7.9$) of its host galaxy, NGC 2366, are at the low end of the reported GP mass and metallicity ranges ([Izotov et al. 2011](#)). Thus, if this system is indeed an LCE, its proximity further suggests that faint LCEs may be commonplace, supporting a significant role in cosmic reionization. Mrk 71/NGC 2366, as a Green Pea analog at a distance of only 3.4 Mpc and LCE candidate, offers an unprecedentedly detailed look at the morphology and physical conditions of a potential LyC emitter.

We thank Nils Bergvall, Norberto Castro, Charles Cowley, Jim Dale, Sergiy Silich, and Linda Smith for helpful discussions. We also thank Kim Sokal for providing us with spectra of Knot A and Knot B. We are also grateful to the anonymous referee for helpful suggestions.

REFERENCES

- Alvarez, M. A., Finlator, K., & Trenti, M. 2012, *ApJL*, 759, L38
 Amorín, R., Pérez-Montero, E., Vílchez, J. M., & Papaderos, P. 2012a, *ApJ*, 749, 185

- Amorín, R., Vílchez, J. M., Hägele, G. F., et al. 2012b, *ApJL*, 754, L22
- Amorín, R. O., Pérez-Montero, E., & Vílchez, J. M. 2010, *ApJL*, 715, L128
- Atek, H., Richard, J., Jauzac, M., et al. 2015, *ApJ*, 814, 69
- Baldwin, J. A., Phillips, M. M., & Terlevich, R. 1981, *PASP*, 93, 5
- Bergvall, N., Zackrisson, E., Andersson, B.-G., et al. 2006, *A&A*, 448, 513
- Binette, L., Drissen, L., Ubeda, L., et al. 2009, *A&A*, 500, 817
- Borthakur, S., Heckman, T. M., Leitherer, C., & Overzier, R. A. 2014, *Science*, 346, 216
- Bouwens, R. J., Illingworth, G. D., Oesch, P. A., et al. 2015, *ApJ*, 811, 140
- Calzetti, D., Armus, L., Bohlin, R. C., et al. 2000, *ApJ*, 533, 682
- Cardamone, C., Schawinski, K., Sarzi, M., et al. 2009, *MNRAS*, 399, 1191
- Corwin, H. G. 2006, Historical Notes: NGC 2000 thru NGC 2999 (Aug, 2006), The NGC/IC Project, http://www.ngcicproject.org/corwin/DataFiles/Aug_2006/ngcnotes_2.txt, Accessed: 2016, March 1
- Cox, N. L. J., Cordiner, M. A., Ehrenfreund, P., et al. 2007, *A&A*, 470, 941
- Crowther, P. A., Schnurr, O., Hirschi, R., et al. 2010, *MNRAS*, 408, 731
- Crowther, P. A., & Walborn, N. R. 2011, *MNRAS*, 416, 1311
- Dale, D. A., Cohen, S. A., Johnson, L. C., et al. 2009, *ApJ*, 703, 517
- de Barros, S., Vanzella, E., Amorín, R., et al. 2016, *A&A*, 585, A51
- de Vaucouleurs, G., de Vaucouleurs, A., Corwin, Jr., H. G., et al. 1991, Third Reference Catalogue of Bright Galaxies. (New York, NY, USA: Springer)
- Dijkstra, M., Gronke, M., & Venkatesan, A. 2016, *ApJ*, 828, 71
- Drissen, L., Roy, J.-R., & Moffat, A. F. J. 1993, *AJ*, 106, 1460
- Drissen, L., Roy, J.-R., Robert, C., Devost, D., & Doyon, R. 2000, *AJ*, 119, 688
- Dufour, R. J., & Harlow, W. V. 1977, *ApJ*, 216, 706
- Esteban, C., Peimbert, M., Torres-Peimbert, S., & Rodríguez, M. 2002, *ApJ*, 581, 241
- Ferland, G. J., Korista, K. T., Verner, D. A., et al. 1998, *PASP*, 110, 761
- Fernandez, E. R., & Shull, J. M. 2011, *ApJ*, 731, 20
- Garnett, D. R., Dufour, R. J., Peimbert, M., et al. 1995, *ApJL*, 449, L77
- González Delgado, R. M., Leitherer, C., & Heckman, T. M. 1999, *ApJS*, 125, 489
- Gonzalez-Delgado, R. M., Perez, E., Tenorio-Tagle, G., et al. 1994, *ApJ*, 437, 239
- Gräfener, G., & Vink, J. S. 2015, *A&A*, 578, L2
- Guaita, L., Pentericci, L., Grazian, A., et al. 2016, *A&A*, 587, A133
- Hawley, S. A. 2012, *PASP*, 124, 21
- Heckman, T. M., Sembach, K. R., Meurer, G. R., et al. 2001, *ApJ*, 558, 56
- Heckman, T. M., Hoopes, C. G., Seibert, M., et al. 2005, *ApJL*, 619, L35
- Heckman, T. M., Borthakur, S., Overzier, R., et al. 2011, *ApJ*, 730, 5
- Henry, A., Scarlata, C., Martin, C. L., & Erb, D. 2015, *ApJ*, 809, 19
- Hoopes, C. G., Heckman, T. M., Salim, S., et al. 2007, *ApJS*, 173, 441
- Hunter, D. A., Elmegreen, B. G., & van Woerden, H. 2001, *ApJ*, 556, 773
- Hunter, D. A., & Hoffman, L. 1999, *AJ*, 117, 2789
- Hunter, D. A., Ficut-Vicas, D., Ashley, T., et al. 2012, *AJ*, 144, 134
- Izotov, Y. I., Guseva, N. G., Fricke, K. J., & Henkel, C. 2011, *A&A*, 536, L7
- . 2014, *A&A*, 561, A33
- Izotov, Y. I., Guseva, N. G., & Thuan, T. X. 2011, *ApJ*, 728, 161
- Izotov, Y. I., Orlová, I., Schaerer, D., et al. 2016a, *Nature*, 529, 178
- Izotov, Y. I., Schaerer, D., Thuan, T. X., et al. 2016b, *MNRAS*, 461, 3683
- Izotov, Y. I., & Thuan, T. X. 2011, *ApJ*, 734, 82
- Izotov, Y. I., Thuan, T. X., & Lipovetsky, V. A. 1997, *ApJS*, 108, 1
- James, B. L., Aloisi, A., Heckman, T., Sohn, S. T., & Wolfe, M. A. 2014, *ApJ*, 795, 109
- James, B. L., Auger, M., Aloisi, A., Calzetti, D., & Kewley, L. 2016, *ApJ*, 816, 40
- James, B. L., Tsamis, Y. G., Walsh, J. R., Barlow, M. J., & Westmoquette, M. S. 2013, *MNRAS*, 430, 2097
- Jaskot, A. E., & Oey, M. S. 2013, *ApJ*, 766, 91
- . 2014, *ApJL*, 791, L19
- Jaskot, A. E., & Ravindranath, S. 2016, *ApJ*, 833, 136
- Kennicutt, R., Balick, B., & Heckman, T. 1980, *PASP*, 92, 134
- Kennicutt, Jr., R. C., Lee, J. C., Funes, J. G., et al. 2008, *ApJS*, 178, 247
- Leitet, E., Bergvall, N., Hayes, M., Linné, S., & Zackrisson, E. 2013, *A&A*, 553, A106
- Leitet, E., Bergvall, N., Piskunov, N., & Andersson, B.-G. 2011, *A&A*, 532, A107
- Leitherer, C., Ekström, S., Meynet, G., et al. 2014, *ApJS*, 212, 14
- Leitherer, C., Ferguson, H. C., Heckman, T. M., & Lowenthal, J. D. 1995, *ApJL*, 454, L19
- Leitherer, C., Hernandez, S., Lee, J. C., & Oey, M. S. 2016, *ApJ*, 823, 64
- Leitherer, C., Tremonti, C. A., Heckman, T. M., & Calzetti, D. 2011, *AJ*, 141, 37
- Lelli, F., Verheijen, M., & Fraternali, F. 2014, *A&A*, 566, A71
- Luridiana, V., Peimbert, M., & Leitherer, C. 1999, *ApJ*, 527, 110
- Madau, P., & Dickinson, M. 2014, *ARA&A*, 52, 415
- Masegosa, J., Moles, M., & del Olmo, A. 1991, *A&A*, 249, 505
- McQuinn, K. B. W., Skillman, E. D., Dolphin, A. E., & Mitchell, N. P. 2015, *ApJ*, 808, 109
- McQuinn, K. B. W., Skillman, E. D., Cannon, J. M., et al. 2010, *ApJ*, 721, 297
- Micheva, G., Iwata, I., Inoue, A. K., et al. 2017, *MNRAS*, 465, 316
- Moustakas, J., & Kennicutt, Jr., R. C. 2006, *ApJS*, 164, 81
- Nakajima, K., & Ouchi, M. 2014, *MNRAS*, 442, 900
- Noeske, K. G., Guseva, N. G., Fricke, K. J., et al. 2000, *A&A*, 361, 33
- Overzier, R. A., Heckman, T. M., Schiminovich, D., et al. 2010, *ApJ*, 710, 979
- Overzier, R. A., Heckman, T. M., Kauffmann, G., et al. 2008, *ApJ*, 677, 37
- Overzier, R. A., Heckman, T. M., Tremonti, C., et al. 2009, *ApJ*, 706, 203
- Peimbert, A. 2003, *ApJ*, 584, 735
- Pellegrini, E. W., Oey, M. S., Winkler, P. F., et al. 2012, *ApJ*, 755, 40
- Pettini, M., & Pagel, B. E. J. 2004, *MNRAS*, 348, L59
- Razoumov, A. O., & Sommer-Larsen, J. 2010, *ApJ*, 710, 1239
- Rigby, J. R., Bayliss, M. B., Gladders, M. D., et al. 2015, *ApJL*, 814, L6
- Rosa, M., Joubert, M., & Benvenuti, P. 1984, *A&AS*, 57, 361
- Roy, J.-R., Aube, M., McCall, M. L., & Dufour, R. J. 1992, *ApJ*, 386, 498

- Roy, J.-R., Boulesteix, J., Joncas, G., & Grundseth, B. 1991, *ApJ*, 367, 141
- Sabbi, E., Lennon, D. J., Anderson, J., et al. 2016, *ApJS*, 222, 11
- Schwartz, C. M., & Martin, C. L. 2004, *ApJ*, 610, 201
- Shapley, A. E., Steidel, C. C., Strom, A. L., et al. 2016, *ApJL*, 826, L24
- Siana, B., Teplitz, H. I., Colbert, J., et al. 2007, *ApJ*, 668, 62
- Siana, B., Shapley, A. E., Kulas, K. R., et al. 2015, *ApJ*, 804, 17
- Smith, L. J., Crowther, P. A., Calzetti, D., & Sidoli, F. 2016, *ApJ*, 823, 38
- Sokal, K. R., Johnson, K. E., Indebetouw, R., & Massey, P. 2016, *ApJ*, 826, 194
- Stark, D. P. 2016, *ARA&A*, 54, 761
- Stark, D. P., Richard, J., Siana, B., et al. 2014, *MNRAS*, 445, 3200
- Stasińska, G., Izotov, Y., Morisset, C., & Guseva, N. 2015, *A&A*, 576, A83
- Steidel, C. C., Pettini, M., & Adelberger, K. L. 2001, *ApJ*, 546, 665
- Thuan, T. X., Bauer, F. E., & Izotov, Y. I. 2014, *MNRAS*, 441, 1841
- Thuan, T. X., & Izotov, Y. I. 2005, *ApJ*, 627, 739
- Tolstoy, E., Saha, A., Hoessel, J. G., & McQuade, K. 1995, *AJ*, 110, 1640
- Vanzella, E., Giavalisco, M., Inoue, A. K., et al. 2010, *ApJ*, 725, 1011
- Vanzella, E., de Barros, S., Castellano, M., et al. 2015, *A&A*, 576, A116
- Vanzella, E., Castellano, M., Meneghetti, M., et al. 2017, *ApJ*, 842, 47
- Verhamme, A., Orlitová, I., Schaerer, D., & Hayes, M. 2015, *A&A*, 578, A7
- Walter, F., Brinks, E., de Blok, W. J. G., et al. 2008, *AJ*, 136, 2563
- Whitmore, B. C., & Zhang, Q. 2002, *AJ*, 124, 1418
- Zastrow, J., Oey, M. S., Veilleux, S., & McDonald, M. 2013, *ApJ*, 779, 76